TURBULENT MIXING IN THE BREAKING ZONE

M.Díez[(1)], Bezerra M. O[(2)], J.P. Sierra[(1)], J.M.Redondo[(2)],

(1): Laboratorio de Ingeniería Marítima LIM,
(2):Laboratorio de Dinámica de Fluidos, Dept. Física Aplicada.
ETSECCPB, Univ. Politecnica de Catalunya, Campus Nord, Barcelona. Spain.

1.Introduction

The breaking zone is the most important case of the surf coastal zone where turbulence is produced. Its study is complex because there are different hydrodynamic processes overlapped: breaking waves, bottom and surface friction, currents, etc. The interaction of several spatial and temporal scales make difficult to separate the scale between several overlapping processes such as turbulence at or near its integral scale and the fastest or shortest waves. In figure 1 we show on a Time vs. Length plot the various basic mechanisms that may contribute to the coastal flow.

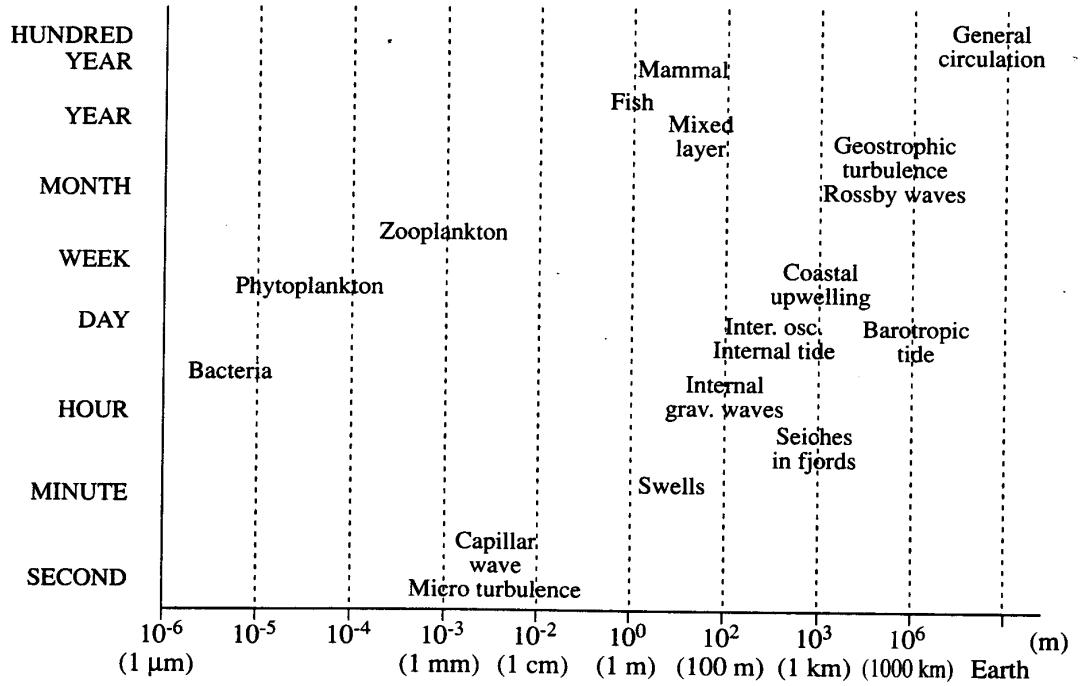

FIG. 1. – Characteristic size range of organisms and physical length and time scales.

However, turbulent mixing itself is a very interesting topic due to its influence in processes such as the transport chemicals in water, sediments, pollutant dispersion, etc.

Video images recorded after the release of dye patches in the experiments carried out has been used to investigate turbulent mixing. The digital analysis technique allows estimate both the spatial and temporal characteristics of a flow. Horikawa et al.(1978), Lippman and Holman (1989) and Ozmidov (1990) have used image analysis to describe the coastal zone using elevated points or balloons to record the images.

Experimental results of horizontal dispersion coefficients in the surf zone under low energy conditions are presented in sections 3 to 5 after a description of the basic theory. Finally we present the conclusions on the different phenomena that cause diffusion in the ocean.

2.Turbulent diffusion

Usually, the dispersive phenomena are modelled by means of the "convection-diffusion equation":

$$\frac{\partial c}{\partial t} + u_i \frac{\partial c}{\partial x_i} = D\nabla^2 c \qquad \text{i, j =1,2,3} \tag{1}$$

Where $\boldsymbol{c}$ is the tracer concentration per unit mass, $\boldsymbol{u_i}$ a velocity component at the position $\boldsymbol{x_i}$ and $\boldsymbol{D}$ the molecular diffusion coefficient assumed isotropic and constant. The first term is the time variation of the concentration; the second one is the advective component and the last one the diffusive component. This equation has some limitations on its applications that arise due to the co-existence of several phenomena at the different spatial and temporal scales.

	TIME	LENGTH
TURBULENCE	$10^{-1} - 10^{-3}$ s	10^{-1} - 10^{-3} m
WAVE FIELD	10^{-1} s - 10 min	1 - 100 m
CURRENT	10 min - 1 h	100 m - 1 km

Table 1 Temporal and spatial scales in the breaking zone.

By means of a statistic analysis devised by Reynolds, a variable $\boldsymbol{u}$ may be decomposed in its mean $\boldsymbol{U}$ and oscillatory components $\boldsymbol{u'}$.

$$u = U + u' \tag{2}$$

Introducing now $\boldsymbol{S_c}$ as a source term of the tracer $\boldsymbol{c}$, the equation 1 becomes:

$$\frac{\partial C}{\partial t} + \frac{\partial c'}{\partial t} + U_i \frac{\partial C}{\partial x_i} + u'_i \frac{\partial C}{\partial x_i} + U_i \frac{\partial c'}{\partial x_i} + u'_i \frac{\partial c'}{\partial x_i} = D\frac{\partial^2 C}{\partial x_i^{\,2}} + D\frac{\partial^2 c'}{\partial x_i^{\,2}} + S_c \tag{3}$$

The problem may be simplified, choosing the adequate temporal and spatial scale to average, the turbulent scale, so some terms could be neglected. The oscillatory components are stationary and uniform Coupled with the mass conservation, the equation can be written as:

$$\frac{\partial C}{\partial t} + U_i \frac{\partial C}{\partial x_i} + \frac{\partial(\overline{u'_j\, c'})}{\partial x_i} = D\frac{\partial^2 C}{\partial x_i^{\,2}} + S_c \tag{4}$$

where the terms dependent on $(\overline{u'_j\, c'})$ indicate that the correlation between velocities and concentration fluctuations play an important role in turbulent transport.

From a similar analyses of Navier-Stokes equation where the turbulent transport is proportional to the velocity gradient:

$$-\overline{u'_i\, c'} = K_{i,j}\frac{\partial C}{\partial x_{i,j}} \tag{5}$$

Being ***K*** the turbulent diffusion tensor of concentration, mass or heat. It is a quantity that depends mostly on the type of flow, but is independent of the fluid characteristics, which are defined on a molecular scale.

, Reynolds derived the now called Reynolds stresses as:

$$\tau_{i,j} = -\rho\,\overline{u'_i\, u'_j} \tag{6}$$

which may be considered as the turbulent transport of momentum.

Boussinesq suggested that the turbulent flux stress is proportional to the mean velocity gradient, in an analogy of the behaviour of the viscosity stress.

$$\tau_{1,3} = \nu_m \rho\frac{\partial u}{\partial z} + \nu'_t\,\rho\frac{\partial u}{\partial z} \tag{7}$$

Being ν_m the molecular viscosity and ν'_t the turbulent viscosity.

Under developed turbulence, the molecular viscosity is several magnitude orders smaller than its turbulent counterpart and it can be neglected. Also the momentum flux in the direction ***i***, of an element that fluctuates in the direction ***j*** could be obtained multiplying the turbulent flux $\rho u'_i$ by $(-u'_j)$. In a time average it is equivalent to the shear stress:

$$\tau = \nu_t \rho\frac{\partial U}{\partial z} = \rho\nu_t\left(\frac{\partial U_i}{\partial x_j} + \frac{\partial U_j}{\partial x_i}\right) - \frac{2}{3}\rho k\delta_{i,j} \tag{8}$$

Being $\delta_{i,j}$ the Kronecker delta and ***k*** the turbulent kinetic energy:

$$k = 1/2\ \overline{u'_i\, u'_j} = 1/2(u'^2+v'^2+w'^2) \tag{9}$$

Considering the above concepts, the diffusion-advection equation becomes a turbulent dispersion equation:

$$\frac{\partial c}{\partial t} + U_i\frac{\partial c}{\partial x_i} = D\nabla^2 C + \frac{\partial}{\partial x_i}\left(K'_{i,j}\frac{\partial c}{\partial x_j}\right) \qquad \text{i, j =1,2,3} \tag{10}$$

where ***K'*** considers only the dispersion effects due to the differential advection so the molecular diffusion ***D*** and the molecular viscosity could be neglected. There is an analogy between the momentum and scalar behaviour (table 2).

Transport of / by	Molecular	Turbulent	Total
Momentum	ν_m	ν'_t	ν_t
Scalar property	D	K’	K

Table 2. Analogy of mass and momentum coefficients.

Obviously, a cloud of tracer grows during the diffusion process, so that its concentration decreases. Considering the analogy proposed by Einstein between the turbulent diffusion and the Brownian movement, this coefficient could be estimated by means of video images analysis of a cloud of tracer accepting a linear relationship between the intensity of the image and the concentration field. Einstein's analogy is only strictly valid in a velocity field with a Gaussian distribution, so is only applicable to clouds with an elliptic shape. In this case, we can calculate the diffusion coefficient in a horizontal direction as a function of the variance of the length in this direction σ^2

$$K_H = \sigma \frac{d\sigma}{dt} = Lu' \tag{11}$$

and we incorporate the additional hypothesis, valid for a limited range of scales that the size of the dye blob standard deviation is comparable with the integral length scale of the local turbulence and that its increase in time is mostly due to the r.m.s. turbulent fluctuations of the velocity field.

Considering K(x,t) constant in time, like in the molecular diffusion, the integral of the equation indicates that the length is proportional to the root square of the time $L \propto t^{1/2}$.

$$K_H t = \frac{1}{2}\sigma^2 \tag{12}$$

In that case u' is constant and the diffusion is produced by the surface friction. Similarly to the wind profile velocity where the relevant velocity is the friction velocity:

$$u'_* = \sqrt{\tau/\rho} \tag{13}$$

In the inertial sub-range the spectra has a power law dependence with the wavenumber between the integral or characteristic scale (L) due some relevant phenomena like the breaking waves or the shear stress of wind or currents, and the smallest eddy scale or Kolmogorov scale (Kolmogorov 1941).

From Kolmogorov´s theory the velocity fluctuations u' depends of the scale as:

$$u' = c\, \varepsilon^{1/3}\, L^{1/3} \tag{14}$$

so when the integral scale is of the same order of the dye cloud $L \approx \sigma$ the Richardson´s law is obtained (Richardson 1922):

$$K_H = Lu' = c\varepsilon^{1/3} L^{4/3} \tag{15}$$

and integrating

$$\int Lu' = \int L \frac{dL}{dt} = \int c\varepsilon^{1/3} L^{4/3} \tag{16}$$

$$-3(L - L_0)^{2/3} = c\varepsilon^{1/3}(t - t_0) \tag{17}$$

So that the spatial dimension grows in time like $L \propto t^{3/2}$.

In turbulent processes with an energy inflow occurring at different scales the relationship $L \propto t^{n/2}$ varies between n=1 (for K = constant) to n=3 (homogeneous turbulence) and for other exponents it is often called anomalous diffusion.

3.Experiments

The visual techniques used in flow analyses are classical tools of the fluid mechanics laboratory experiments. The breaking zone conditions are very difficult to reproduce in the laboratory so it is necessary to measure "in situ" during field campaign experiments (Such as those within the frame of the European projects MAST and FANS and the C.C.D.).

The field experiments were carried out in three different sites:

* Two campaigns were made in the Trabucador's Bar in the Ebro Delta, in December 1993 and November 1996 (see figure 2). On this site usually there are strong longshore currents, uniform behaviour and a multibarred profile.

*A series of measurements were also taken during 1994, 1995 and 1996 at St Gervasi Beach in Vilanova i la Geltrú, near Barcelona. This is a 240 m length beach, enclosed in the middle of two large boulder wavebreakers. The longshore circulation develops only with high waves and two or more cells produce recirculation between the wavebreakers (Bezerra et al. 1995).

*Another study site was the Olinda beach, close to the harbour of the city of Recife in Brazil, where wind and tidal effects became very important. See (Bezerra 1999).

Campaign	Ebro'93	Ebro'96	Vilanova	Recife
N^{er} Experiments	7-9	8	8-10	40
Wind speed (m/s)	0-10	0-15	0-10	0-25
Wave height (m)	0.1-0.75	0.1-0.5	0.1-2	0.5-3
Current speed (m/s)	0-1.5	0-0.65	0-0.1	0-3

Table 3. Number of experiments performed with range of environmental parameters

Video images and hydrodynamic velocities time series were simultaneously measured, allowing further correlative analysis of hydrodynamics and mixing processes. The images were recorded with remote video cameras in different places: a crane with an arm of 40 m long, hanged to an aerostatics balloon, allowing a zenithal view of study area, high buildings and street lamps. In table 3 the number of different experiments performed and analysed here are indicated together with the measured range of wind speeds at 2 m , of maximum wave heights and surface current speeds.

In these experiments, milk and/or fluoresceine, rhodamine, MnO_4K_2, SO_4Ca and others were used as tracers. The best contrast and persistence for video recording were obtained with a solution of milk and fluoresceine. All the released clouds were of the same volume of tracer in order to compare the results at similar sizes.

Figure 2. Ebro Delta experiment showing a blob of dye and the velocity measurement station.

4. Data processing

We obtained quantitative information from video images using the *DigImage* video analysis system, and arithmetic frame grabbers DT2861, which allows a resolution of 512 by 512 pixels and 256 grey levels (Dalziel, 1994).

The surf zone images analysis needed several previous manipulating processes such as co-ordinate transformation, filtering the noise in the image, avoiding the background, images average and others, depending on the kind of light field, image quality and physical phenomena to b studied.

Once the images are digitally filtered, it's possible to follow the spatial and temporal evolution of the dye spot, thus, obtaining the dispersion coefficient.

The methodology used to obtain the coefficients is explained in detail in Rodriguez et al. (1997a) and in Bezerra et al.(1998). As an example in figure 3, from Bahia (1997) the digital enhancement performed on a detected dye blob allows even to investigate the anisotropy of the dispersion

There are two basic methods to find the coefficient of turbulent diffusivity after measuring the evolution of the size of the blob in time $\sigma = \sigma(t)$.

A) From a gaussian fit to the longshore and crosshore components of the dye blob calculate the variance and apply directly Einstein´s equation.

B) Find directly the rate of growth of the blob size and multiply this rate times the standard deviation of the gaussian fit to the dye blob.

In figure 3 a sequence of digitalized intensity profiles of the blob of dye (milk) is shown. Taking care to identify the background level of reflected light intensity and

correcting for possible changes in the light conditions, the gaussian fit is simple even in relatively complex shapes. The two methods mentioned above correspond to using one of the two equivalent equations:

$$K = \tfrac{1}{2}\frac{d\sigma^2}{dt} = \sigma \cdot \frac{d\sigma}{dt}. \qquad (18)$$

Image of a dye spot

Matrix of intensities

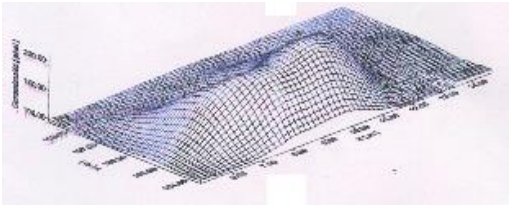

3D Plot of intensities field

Map of intensity

Figure 3. Sequence of study of video images

5. Results

In the surf zone the turbulent eddy dispersion coefficients may vary more than an order of magnitude for the same wave conditions depending on the breaking conditions, the distance from the shoreline and the profile of the longshore current.

Comparing breaking and non-breaking waves, the breaking waves diffusivity are often larger, the anisotropy defined as the ratio between longitudinal and transversal variances of the blob size and is also larger for breaking waves Bahia (1997). Other parameter indicating anisotropy used here is the ratio of longshore to crosshore eddy diffusivity K_x / K_y .

In the Ebro Delta experiments, the range of transversal dispersion coefficients were between 0.005 and 0.6 m^2/s. The minimum values are slightly larger than the case of

Vilanova (0.001 to 1 m^2/s) because it is a confined beach with no longshore current, but the maximum values are due to the different weather conditions. The range of diffusivities from the Recife and Olinda experiments is between 0.002 and 1 m2/s, but there the tidal currents were also important.

In order to estimate the effect of the waves on the turbulent eddy diffusivity, ***K***, we use a Reynolds number of the flow induced by the wave as:

$$Rw = H\,V / \nu \tag{19}$$

Where ν is the cinematic viscosity of seawater**,** ***H*** is the wave height and ***V*** is the orbital velocity $\boldsymbol{V = H / T,}$ with ***T*** the average period or the wave phase speed $\boldsymbol{V = \lambda / T,}$ with $\boldsymbol{\lambda}$ the average wavelength.

The difference between both ways of estimating the relevant velocity producing the stirring depends on $\boldsymbol{\tan\alpha = 2H / \lambda}$ which will vary if the waves are breaking or not. This will also function of the depth ***D*** and the criteria of wave breaking. For very shallow waters, it may be approximated by :

$$V = \sqrt{g(H + D)} \tag{20}$$

In most cases we have used:

$$Rw = \frac{2H^2}{\tan\alpha T\nu} = \frac{\tan\alpha\lambda^2}{2T\nu} \tag{21}$$

From video image analysis the wave period may be easily found as well as the wavelength. The evolution of the wave frequencies with cross-shore distance was studied using time series and the agreement with the DWR was also good (Rodriguez et al, 1997).

The eddy diffusivity values are plotted against the wave Reynolds number and it show an increase of K_l between 10^3 and 10^6, for higher Rw other effects are more important, such currents or wind. These results for all the experimental sites are shown in figure 4 where the closed symbols indicate crosshore values and the open ones indicate longshore or parallel to the coast components of the diffusivity.

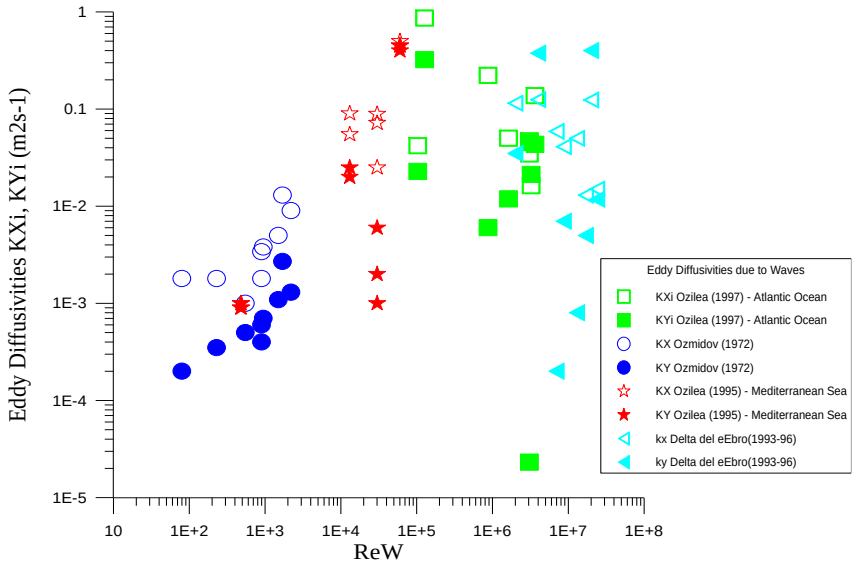

Figure 4. Eddy diffusivity longshore and crosshore

The presence of currents and shear tends to elongate the blobs, this explains the low diffusivity values at ***Rw*** = 3 10^4 and at Rw = 10^7. In figure 5 these effects are seen more clearly, for low ***Rw*** most dye blobs are isotropic but as larger waves induce a strong vorticity component parallel to the shoreline the anisotropy increases to values up to 1000. The few cases that exhibit values less than one are due to strong rip currents.

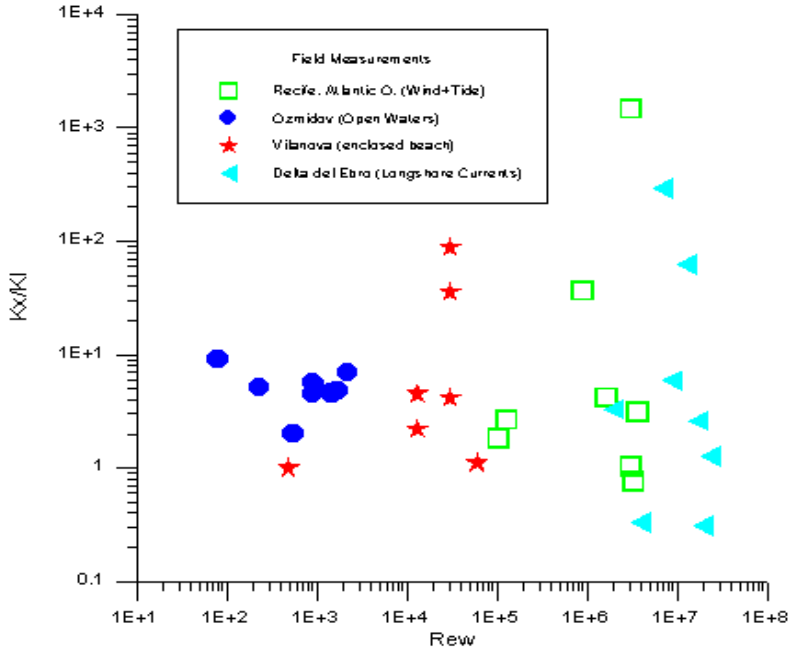

Figure 5. Anisotropy of diffusivity coefficients.

In figure 6 we show an example of different shapes of dye intensity measured as the blob of dye moves using an absolute spatial reference level. One effect observed is the oscillatory motion suffered by the dye as waves pass through it.

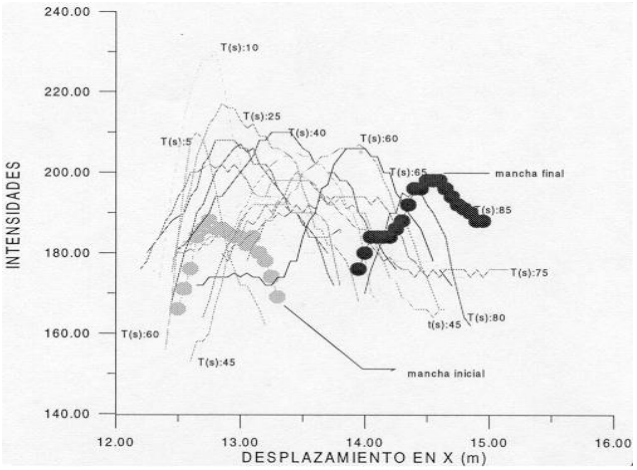

Figure 6. Intensity sections at different times.

In figure 7 we compare the values of the eddy diffusivities for the sites of Vilanova (fig 7 a) and of Recife (fig 7 b). We note that the larger wave heights of Recife and the additional effect of tidal induced currents preclude any correlation.

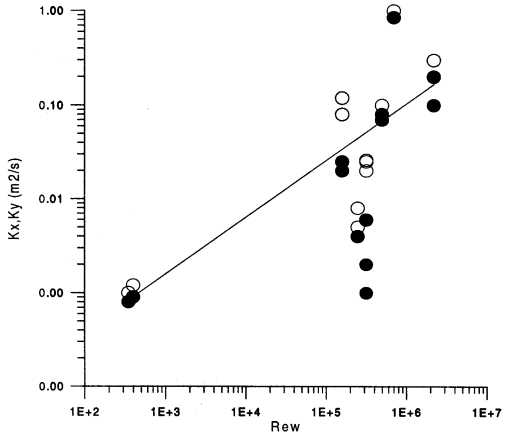

Figure 7 a) Vilanova i la Geltru experiments.

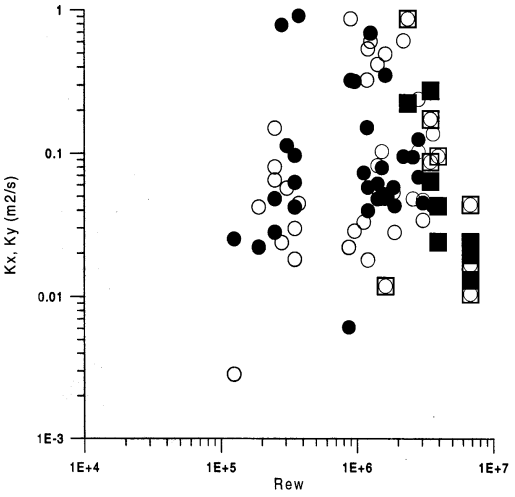

Figure 7 b) Recife (Olinda) experiments.

5.1 Effect of wind stress on horizontal diffusion

For Vilanova i la Geltru data, also show in figure 7 a) we also calculated wind stress evaluations the friction velocities $\boldsymbol{u}_*$ from the logarithmic wind profiles such as that shown in figure 8. We can see there in the same plot the data corresponding to the mean wind (circles) and their r. m. s. fluctuations (crosses) for a low wind experiment, about 3 m/s at 3m height just at the shoreline.

An interesting observation that is repeated in most cases with strong waves is the departure from the standard logarithmic wind profile at heights smaller than the average wave height (0.5 m) in that particular experiment. In spite of this excess low level momentum due to the interaction between wind and waves the extrapolation of the

semilogarithmic plot to V=0 defines the roughness height z_0. The behaviour of the fluctuations near the sea surface also indicates that the level of the friction velocity which may be calculated as proportional to the slope in figure 8, or directly from:

$$U(z) = \frac{u_*}{k} \ln(\frac{z}{z_0}) \tag{22}$$

where ***k*** is von Karman's constant (k=0.42) and ***z0*** is the friction lengthscale that may be evaluated from plots such as the one shown in figure 8. The average wind values and the root mean square of turbulent wind fluctuations are plotted. The Reynolds stress τ may be evaluated from the friction velocity as:

$$\tau = \rho u_*^2 \tag{23}$$

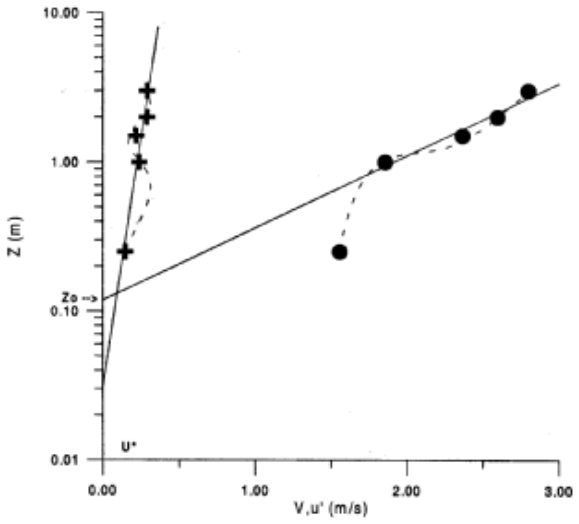

Figure 8. Evaluation of the Logarithmic wind profile from data

The different physical mechanisms at the different sites play a different role in each of them, for example in the Ebro Delta data, one of the dominant effects is the persistency of a longshore current that together with the wave breaking due to an underwater sand bar also gives a strong parabolic dependence of the diffusivity with distance from the coastline as shown in Bezerra et al.(1998). In the Recife experiments in the southern Atlantic, the effect of tidal currents is also important but is not taken into account explicitly here.

6. Discussion and conclusions

We have seen that the larger the wave height, the stronger the anisotropy exhibited by the eddy diffusivity, this is to be expected due to the strong production of horizontal vorticity parallel to the sea surface and perpendicularly to the wave speed. The mixing there is much more pronounced if the waves do break.

A strong correlation between the values of eddy diffusivity and wave height represented in terms of a wave dependent Reynolds number is only possible for the experiments performed in abscence of longshore or tidal currents. A power law may be deduced in the range of values of R_w between 10^2 and 10^6 as $K_x = c\, R_w^{4/5}$.

The effect of the wind acting in combination to the waves may be seen very clearly in figure 9, there the different conditions for the experiments performed in Vilanova are plotted showing both the value of u_* and of R_w. We see that most data appear in a straight line indicating a natural dependence between wind stress and wave height but there are two other regions in parameter space that may be classified as follows:

a) The data in the upper-left corner is the case with low wind but high waves (swell) indicating propagation of waves from a recent and sometimes distant storm.

b) The data in the lower-right corner are from the initially calm days where a strong wind starts to blow and there is a time lag between the start up of the wind and ripples in the surface and the build up process of wave generation.

The different sites need to be further studied and the other aspects that are relevant in the breaking zone have to be assesed. The influence of currents is presently under way; but from the present data it is clear that both wind and wave action are important in all cases.

Figure 9. Relationship between wind stress and Wave Reynolds Number
for the Vilanova experiments

7. Acknowledgements

We would like to acknowledge support from European Union contracts CT950037, CT950016 and CT960049 MAST III as well as INCO-COPERNICUS (EU-950016) and INTERCAMPUS the contract with CCD for the study of Suape harbour (Brazil).

References

Bahia, E. (1997). Estudio Numérico-Experimental de la Dispersión de Contaminantes en Regiones Costeras, PhD Thesis, Universidad Politécnica de Cataluña, Barcelona.

Dalziel S. DigImage, Image Processing for Fluid Dynamics. Cambridge Enviromental Reserch Consultants Ltd. March 1994.

Horikawa, K., Lin, M.C., Sasaki, T.O. (1978). Mixing of heated water discharged in the surf zone. I.C. Coastal Engineering, ASCE, 2563-2583.

Kolmogorov A. N. (1962) A refinement of previous hypothesis concerning the local structure of turbulence in a viscous incompresible fluid at high Reynolds number. J. Fluid Mechanics 3, 81-85.

Lippmann, T. and Holman, R. (1992). Wave group modulations in cross-shore braking patterns, ICCE, ASCE, 918-931.

Masch, F. D. (1963). Mixing and Dispersion of Wastes by Wind and Wave Action. International Journal of Air Water Poll., vol. 7, pp 697-720.

Ozmidov, R. (1990),Diffusion of contaminants in the ocean. Oceanographic Sciences Library, vol. 4, Kluber Academic Publisher, London.

Redondo J., Rodriguez A., Bahia E., Falqués A., Gracia V., Sánchez Arcilla A. and Stive M.J.F. (1994). Image Analysis of Surf-Zone Hydrodynamics. Coastal Dynamics'94, ASCE.

Richardson L. F. (1922) Weather prediction by numerical processes. C. U.P.

Rodriguez A., Sánchez-Arcilla A., Redondo, J.M., Bahia E. and Sierra, J.P. (1995): Measurements and modelling of pollutant dispersion in the nearshore region, Water Science and Technology, IAWQ, 32, 10-19.

Rodriguez A. (1997). Estudio Experimental de la Hidrodinámica de Zona de Rompientes. PhD Thesis. Laboratori d'Enginyeria Marítima, Escola Técnica Superior de Enginyers de Camins Canals i Ports de Barcelona, Universitat Politècnica de Catalunya.

Rodriguez, A., (1997a) Study of Surf-Zone Mixing Using Video Images. International Conference on Coastal Engineering. ASCE, UK.

Rodriguez, A.; Bahía, E.; Díez, M.; Sánchez-Arcilla, A.; Redondo, J. M. and Mestres, M.. (1997b). Estudio Experimental de Procesos de Mezcla en Aguas Costeras. IV Jornadas Españolas de Ingeniería de Puertos y Costas, Cádiz.

Sánchez-Arcilla, A., Rodriguez, A., Santás, J.C., Mösso, C., Gracia, V., Sospedra, J., K'osyan, R. and Kuznetsov, S. (1997). Experimentos Hidro-morfodinámicos en la zona costera del Delta del Ebro. IV Jornadas Españolas de Ingeniería de Puertos y Costas, Cádiz.

Ziedler, R. (1976). Coastal Dispersion of Pollutants. Journal of Waterways, Harbour and Coastal Engineering, ASCE, vol. 102, ww2 (May), 235-254.